

ANTAL KERPELY DOCTORAL SCHOOL OF MATERIALS SCIENCE & TECHNOLOGY



MISKOLCI
EGYETEM
UNIVERSITY OF MISKOLC

High-Temperature Corrosion Resistance Investigation of Hot-Dip Aluminized Carbon Steel C45

A PhD Dissertation Submitted in Fulfillment of the Requirements for the Degree of Doctor of
Philosophy in Material Science and Engineering

By

Hawkar Jalal Muhammed

Supervisor:

Prof. Dr. Tamás I. Török (Emeritus Professor)

Head of the Doctoral School

Prof. Dr. Valéria Mertinger

Institute of Chemical Metallurgy and Foundry Engineering

Faculty of Materials and Chemical Engineering

University of Miskolc, Hungary

Miskolc

2023

Abstract

The current research employs the hot-dip aluminizing (HDA) process to coat carbon steel C45 with commercially pure aluminum. The primary focus of this investigation is to examine the structural characteristics that develop during the interaction of liquid aluminum and solid C45. The study also explores the influence of an interlayer (precoat copper on C45) on the preferential growth of Fe_2Al_5 . The results indicate that the interlayer reduces the growth of Fe_2Al_5 to $0.646 \mu\text{m}^2 \cdot \text{s}^{-1}$ or $(6.46 \times 10^{-13} \text{ m}^2 \cdot \text{s}^{-1})$, and the layer thickness can be reduced to about $4 \mu\text{m}$ for a shorter dipping time of 45 s. Additionally, the study conducts a high-temperature corrosion test in a cyclic exposure to hot air at $700 \text{ }^\circ\text{C}$. The results show that during cyclic exposure, a dense and compact interdiffusion layer is formed, which is free of oxide and represents the FeAl phase. The examination of HDA C45 is also carried out in harsh environments where the specimens are half-immersed in molten salt mixtures of NaCl and Na_2SO_4 at $700 \text{ }^\circ\text{C}$. The structural characterization reveals severe deterioration due to oxychlorination, which causes rapid corrosion of the coated samples.

Furthermore, the HDA C45 specimens are exposed to different high temperatures ranging from $700 \text{ }^\circ\text{C}$ to $1000 \text{ }^\circ\text{C}$ for different exposure periods of 8, 24, and 72 hours. The results suggest that the optimal working temperature for HDA C45 is $700 \text{ }^\circ\text{C}$ or below in hot air, where less to no severe damage can be detected or seen.

1. Introduction

Operating metallic base materials in most structural components is still a practical matter. These materials have superior mechanical and physical properties, which are the primary reasons behind their application. Examples of structural components include incineration, heat exchangers, power stations, and turbine blades.

A metallic material functioning in high-temperature environments requires special features, such as corrosion resistance, that enable it to operate in these harsh environments without rapidly degrading and failing catastrophically. In order to overcome the abovementioned problem, alloying the metals, first of all, the iron base alloys, with elements such as Cr, Ni, Al, and Si is considered a viable solution, as these elements have stable, protective oxide layers that act as a barrier and mitigate against the flow of oxygen as well as other corrosive agents to the base metal. In this context, a recent focus has also been placed on high-entropy alloys. Alternatively, a suitable coating and/or surface modification, such as surface alloying, can be

applied to protect the base metal component. There are a variety of coating techniques, such as PVD, CVD, HVOF, HDA, HDG, etc. However, it is important to note that the usage of these techniques depends on several factors, such as cost, the level of quality or the purpose of the coating, the type of protective layer/substance, and the type of substrate/base component to be used.

Temperature ranges from low to high, and extremely high temperatures can be used to categorize operating environments. Specifying the proper metallic base material according to the operating temperature is essential. Some possible metal type usage versus working temperatures are worth mentioning, like those low-alloy steels, which form M_3O_4 ($M=Fe, Cr$) surface layers/scales, and are used to temperatures of about or below 500 °C in hot air. Titanium-base alloys form TiO_2 and are used up to about 600 °C. Ferritic stainless steels, which form Cr_2O_3 surface layers, are used to about 650 °C. Austenitic Fe–Ni–Cr alloys, which form Cr_2O_3 surface layers, are used to about 850 °C. Austenitic Ni–Cr alloys, which form Cr_2O_3 surface layers, are used to about 950 °C. Austenitic Ni–Cr–Al alloys, aluminides, and $MCrAlY$ ($M = Ni, Co, or Fe$) coatings, which form Al_2O_3 surface layers, are used to about 1100 °C. Applications above 1100 °C require the use of ceramics or refractory metals.

For decades, scientists/researchers have attempted to understand, explore, and illustrate the oxidation/corrosion phenomena at elevated temperatures. Interactions, diffusion, structural changes, phase changes, intermetallic evolution, and interfacial reaction have been the primary focus of their research. To manage the component's performance and real operating lifetime, continuous study is necessary to assess the metal base material intended for use in high-temperature environments, either bare or coated.

One of the key advantages of hot-dip aluminizing (HDA) is that it provides superior corrosion resistance at high temperatures owing to the formation of a stable aluminum oxide layer that prevents corrosion from damaging the base metal, besides the simplicity and cost-effectiveness. The primary purpose of this PhD program and research work was to use an inexpensive iron base metal, that was the carbon steel C45, coated with the most straightforward and inexpensive coating technique, i.e., HDA. During the PhD research period of several years, first, setting up the necessities to perform laboratory HDA experiments was achieved, where preparations included the molten bath consisting of commercially pure aluminum as well as the preparations of the steel specimens for coating. Then, sophisticated metallographic technology available at the University of Miskolc, Faculty of Material Science and Chemical Engineering, was employed to characterize the morphologies, structures, and mechanical properties and reported accordingly. Afterward, several corrosion resistance examinations were designed and utilized

to investigate the structural changes of HDA carbon steel C45, corrosion kinetics, and imitate the same conditions as the actual component serving. Before HDA, attempts were made to pre-coat the specimens, followed by a structural evaluation to reveal the precoat layer's effect on the intermetallic layer's evolution at the interface. All are reported in this PhD dissertation, and appropriate explanations and discussions are provided with firm and possible causes of the changes.

2. Literature review

2.1 Corrosion

Corrosion is an inevitable process that inflicts significant harm to structures and materials through its reaction with the surrounding environment. This harmful process leads to the generation of compounds such as oxides and salts that significantly impact various industries, including transportation, infrastructure, manufacturing, and energy production. Globally, corrosion has a tremendous economic impact, estimated to be several trillions of Euro/Dollars per year [1].

Corrosion can manifest itself in different forms on metal surfaces, including uniform, pitting, crevice, and galvanic. It's important to note that various factors contribute to corrosion, such as the type of material, the environmental conditions, and the presence of contaminants. These factors significantly influence the extent and severity of corrosion [2,3].

2.2 High temperatures oxidation in air

High-temperature oxidation occurs when materials are exposed to high temperatures in the presence of oxygen. This reaction leads to the generation of oxide layers on the material's surface, which can significantly impact its properties. Industries such as aerospace, power generation, and metallurgy are highly concerned with this process because it can have diverse impacts on the efficiency and reliability of components and structures operating at high temperatures. This is particularly crucial in the aerospace industry.

Equation (1) (where (M) represents a metal) in itself does not yet demonstrate the complexity of the oxidation process. It is crucial to note that a higher temperature accelerates the reaction rate, leading to the formation of oxide layers at a faster rate. Various factors, including the composition of the material, temperature, and partial pressure of oxygen heavily influence the properties of the oxide layer.



Numerous techniques have been devised for analyzing high-temperature oxidation, such as thermogravimetric analysis, X-ray diffraction, and scanning electron microscopy. These methods offer valuable glimpses into the oxide layers' characteristics and facilitate comprehension of oxidation mechanisms.

Materials used in high-temperature applications face a significant challenge in oxidation at high temperatures. Oxide layers can adversely affect their mechanical, thermal, and electrical properties, leading to a drop in performance and early failure. As a result, it is crucial to comprehend the oxidation mechanisms and create effective preventive measures in order to guarantee safe and dependable functioning in high-temperature applications [4,5].

2.3 High temperatures corrosion in molten salt

Iron-based materials used in structural engineering are frequently subjected to high-temperature environments, including gases, melts, and particles in power plants, waste incinerators, and chemical processing plants. This exposure causes the materials to absorb and transfer heat from their surroundings, leading to degradation, such as surface scale formation in hot air. Corrosion processes, including oxidation, are also accelerated by time and temperature fluctuations. Elements such as chlorine, sulfur, sodium, and vanadium often exacerbate corrosion degradation, particularly at high temperatures [4]. Due to aggressive chemical components reacting with surfaces, the formation of new corrosion products, or new scale, weakens the adhesion and permits corrosion species to penetrate and react with the matrix. These processes also produce mechanical stresses that, when coupled with attacks, will severely compromise the components' performance and potentially lead to failure [4].

Corrosion at high temperatures is an extremely critical engineering issue requiring utmost care before utilizing any material component. Many studies have been carried out to examine closely the subject impact of various harsh environments simulated at elevated temperatures on different carbon steels [6] as well as the impact of chlorine on bare carbon steel [7] when corrosion accelerates due to cyclic oxychlorination. Iron oxides (Fe_xO_y) can spall off and weaken the components as iron oxidizes. The degradation of dual-phase steel substrates was observed to occur even at low temperatures using a chloride-based solution [8]. The production of a passive protective film is crucial for achieving sustainable performance in high-temperature environments. Elements such as aluminum and chromium serve as exceptional examples in this regard [9].

The examination of the corrosion and oxidation behavior of high alloy steels and stainless steels with exceptional heat and corrosion resistance has been conducted at high temperatures in the presence of sulfur and chlorine in various forms, including gases, deposited salts, or molten salts [10-16]. Furthermore, in the case of special coatings, such as aluminizing [17,18], to enhance the durability of steel components in extreme environments, it is crucial to reduce the rate at which they degrade. However, it is worth noting that protective measures and techniques are susceptible to deterioration, which is often influenced by kinetic factors, diffusion rates, and thermodynamics. For instance, it has been proven that deposited salt mixtures, such as NaCl and Na₂SO₄ in varying concentration ratios, can significantly accelerate the corrosion of low-carbon steel [7], and the chloride and sulfur present cause corrosion.

3. Scientific goals

The study of hot-dip aluminizing carbon steel C45 aims to advance our fundamental understanding of this specialized coating process and its underlying mechanisms and develop more effective and optimized coating solutions. This objective encompasses a range of goals that seek to uncover the intricate details of the process, characterize the resulting coatings, and leverage this knowledge to enhance material properties for multiple applications. The primary scientific goals are as follows:

1. **Mechanistic Insights:** Researchers must investigate the fundamental mechanisms governing the intermetallic compound formation and the interaction between the aluminum coating and the substrate material during hot-dip aluminizing. It is imperative to understand the kinetics, diffusion pathways, and reactions involved to elucidate the processes that shape the resulting microstructure and properties of the coatings.
2. **Microstructural Understanding:** It is imperative that a thorough comprehension of the microstructural evolution within hot-dip aluminized coatings is achieved. The characterization of the morphology, composition, and distribution of intermetallic phases formed at the coating-substrate interface and throughout the coating's thickness is essential for establishing a correlation between microstructure and performance attributes.
3. **Property-Structure Relationships:** Establishing unequivocal connections between microstructural features and the mechanical, corrosion, and oxidation properties of hot-

dip aluminized coatings is imperative. Researchers must quantify the influence of various microstructural characteristics on different performance metrics to steer the design of coatings with customized properties.

4. **Optimization Strategies:** Developing systematic strategies to optimize the hot-dip aluminizing process for specific applications is imperative. A thorough investigation of the influence of process parameters, including temperature, immersion time, and aluminum alloy composition or interlayer, is necessary to identify conditions that yield coatings with desired attributes.
5. **Functional Tailoring:** Examine potential avenues for customizing the features of hot-dip aluminized coatings to suit particular purposes and uses. Thoroughly scrutinize how modifying alloy composition, coating thickness, and microstructure can be intentionally utilized to amplify resistance to corrosion and high-temperature resilience.

4. Experimental sections

4.1 Substrate material and sample preparation

The substrate material for this study was carbon steel C45 see Table 1. During the preliminary characterization stage, samples were cut from a C45 bar with a diameter of 32 mm and a thickness of 5 mm. The samples were ground using SiC emery paper ranging from 220 to 800 grit and then polished with a diamond wax stick applicator DP-stitch P, 3 μ m from Struers ApS®. DP lubricants were utilized along with a 200 mm woven wool MD-Mol™. Later, the dimensions of the specimens were modified to 10x10x5 mm.

4.2 Liquid bath

The coating was conducted using commercially pure aluminum, which has a chemical composition as shown in Table 1.

Table 1. Constituting major chemical elements of steel C45 specimens and the commercial aluminum bath used in the laboratory HDA experiments.

C45 steel elementary composition (obtained by spectroscopic analysis), wt %									
C	Mn	Si	Cu	Ni	Cr	Mo	S	P	Fe
0.44	0.52	0.18	0.22	0.09	0.08	0.02	0.03	0.01	Rest
Aluminum melt elementary composition (obtained by spectroscopic analysis), wt%									
Fe	Mn	Si	Cu	Zn	Ti	Ni	Ga	Mg	Al
0.92	0.55	0.12	0.08	0.18	0.05	0.02	0.06	0.01	Rest

4.3 Fluxing

Salt mixtures containing (KCl + NaCl + 4% CaF₂) were utilized as a flux layer over the molten aluminum. It was observed through thermogravimetric analysis measurements that the melting point of the prepared salt mixture was lower than that of aluminum.

Later on, the C45 samples were treated with solder flux paste type (EN 29454-1 1.1.2.C) before immersion in liquid aluminum to enhance their adhesion and wettability.

4.4 Coating process

The coating process was conducted through a hot dipping process, as depicted in the accompanying Figure 1.

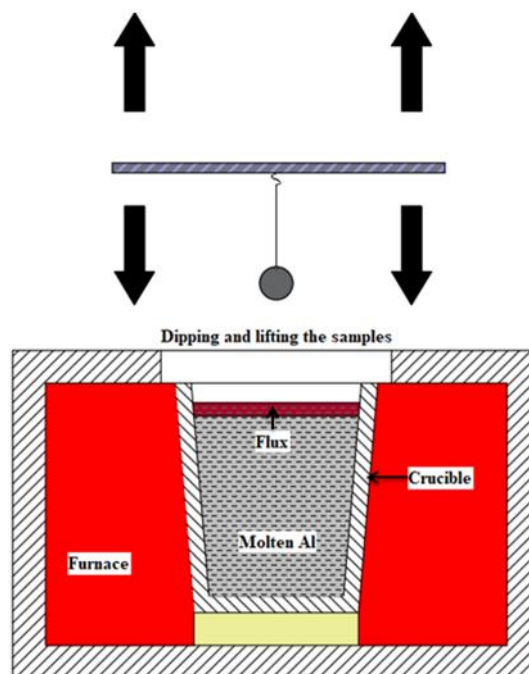


Figure 1. The schematic process illustrates the way conducted to HDA carbon steel C45 specimens.

4.5 High-temperature corrosion examinations

The high-temperature corrosion tests were carried out in three different manners as follows:

1. Cyclic exposure, where the HDA C45 was kept inside a furnace under static hot air at 700 °C for 8 h, then kept inside a furnace that was switched off for 16 hours to allow it to return gradually to the ambient temperature. This cycle was repeated thrice.

2. The HDA C45 was subjected to a series of experiments involving immersion in molten salt mixtures of NaCl + Na₂SO₄ at a temperature of 700 °C. These experiments were conducted under static conditions inside a furnace for three different exposure periods: 8, 24, and 72 h.
3. The endurance of HDA C45 has been examined under varying temperatures of 700, 800, 900, and 1000 °C, with each temperature subjected to exposure periods of 8, 24, and 72 h, respectively.

4.6 Investigation methods

The investigation of the structure features was primarily carried out through the application of metallographic analysis techniques. A Zeiss Evo MA10 scanning electron microscope (SEM) equipped with an energy dispersive spectrometer (EDS) and a Thermo Scientific Helios G4 PFIB CXe type of SEM combined with EDS using a lanthanum hexaboride (LaB₆) emitter were utilized to analyze the structures of cross-sections. For further evaluation of the PFIB SEM images, Orientation Imaging Microscopic (OIM) software was used to analyze each phase's grain size and fraction distribution. An optical microscopic ZEISS Axioscope was used to reveal the structural changes. Further, glow discharge optical emission spectroscopy (GD-OES) GD-profile 2TM from HORIBA was employed to show the distribution profile of the elements developed in the topcoat layer and interdiffusion zone during hot-dipping.

5. Results and discussions

5.1 Structure characteristics of HDA C45

The aluminized samples always showed a layered structure, as is seen in the optical microscopic image in Figure 2. The structure of the aluminized C45 steel specimens exhibits three distinct layers in their cross sections: an aluminum top layer, an intermetallic layer, and a steel substrate. In Figure 2, the form of the intermetallics grown toward the substrate seems to show a tongue or a finger-like structure, which is consistent. Fe–Al intermetallics also appear to be found in the topcoat layer and are spread as needle-like (acicular) crystals see Figure 3. Voids, gaps, and cracks can also be observed, resulting from inclusions incorporated from the molten bath and the intermetallic layer's inherent brittleness Figure 3. Moreover, some small broken fractions even fell out during the saw machine's sectioning of the aluminized sample.

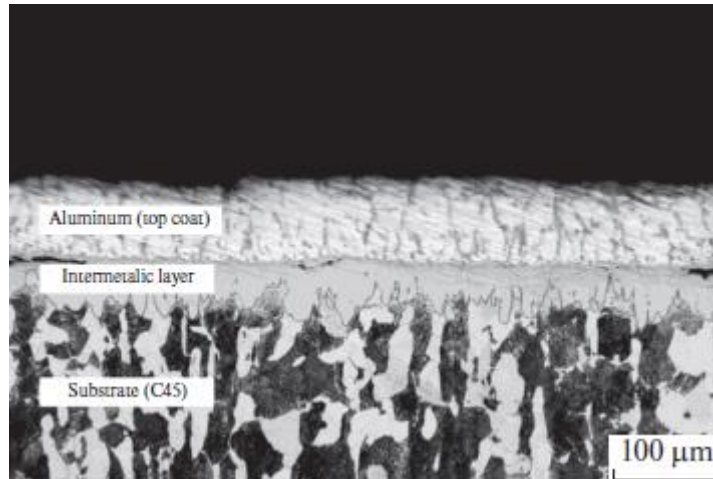


Figure 2. Optical microscopic image of microstructure of aluminized C45 highlighting grains of ferrite (white) and perlite (black) of the steel substrate.

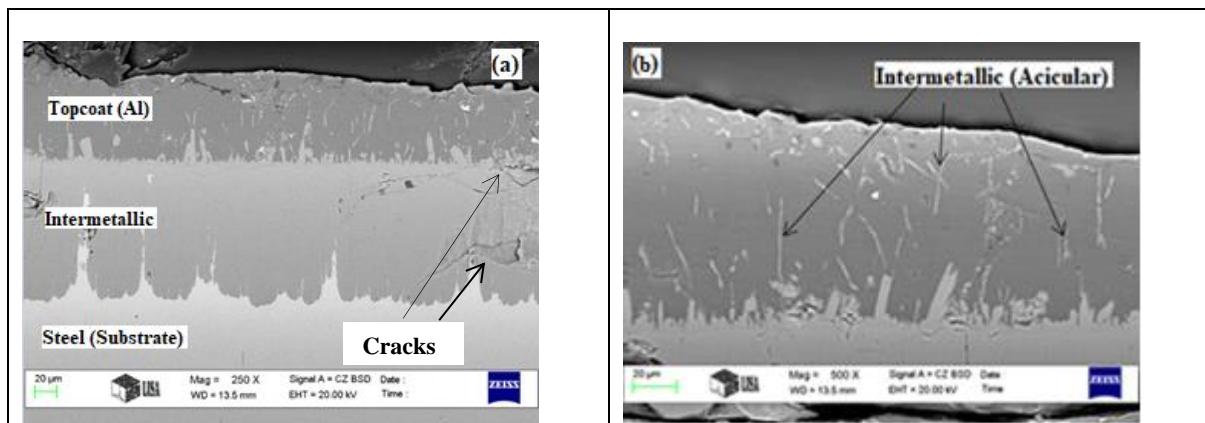


Figure 3. Top of the carbon steel C45 substrate with two distinct layers (a), traces of intermetallic phases in topcoat (Al) (b)

5.2 Structure characteristics of HDA C45 copper precoat

Copper was electroplated onto carbon steel C45 specimens before HDA using a solution containing ($\text{CuSO}_4 \cdot 5\text{H}_2\text{O} + \text{H}_2\text{SO}_4$) diluted in distilled water. The HDA carbon steel specimens were ground and polished for use in structural investigation. The cross-sectional view of each specimen dipped in molten aluminum at different times is shown in Figure 4 (a), (b), (c), and (d), respectively. Overall, the cross-sectional structures are similar, consisting of an aluminum topcoat layer at the top, solidified Fe-Al phases within the topcoat layer ranging in form from flake to acicular shapes, and an intermetallic layer in the middle, in addition to the substrate and its relevance with previous studies. Two phases of the intermetallic layer can be distinguished by color contrast: light gray closer to the substrate and gray towards the topcoat layer. Figure 4(a) shows that the structure of the sample dipped for 45 seconds shows consistent growth; even slightly, there are no indications of microcracks. In addition, no presence of copper could be observed within the intermetallic layer.

However, its existence was confined to the topcoat layer of aluminum, where it was trapped. With the dipping time of 85 seconds, as shown in Figure 4(b), the intermetallic layer's irregular growth finger-like morphology is observed with the initiation of microcracks. Copper could not be detected either in the intermetallic or topcoat layers. As the dipping time increases to 150 s, Figure 4(c), the irregular growth becomes dominant, and the intermetallic layer thickness increases. For a dipping time of 300 s, Figure 4(d), irregular growth becomes disorderly. Furthermore, copper was not detectable in either sample; cracks are clearly visible.

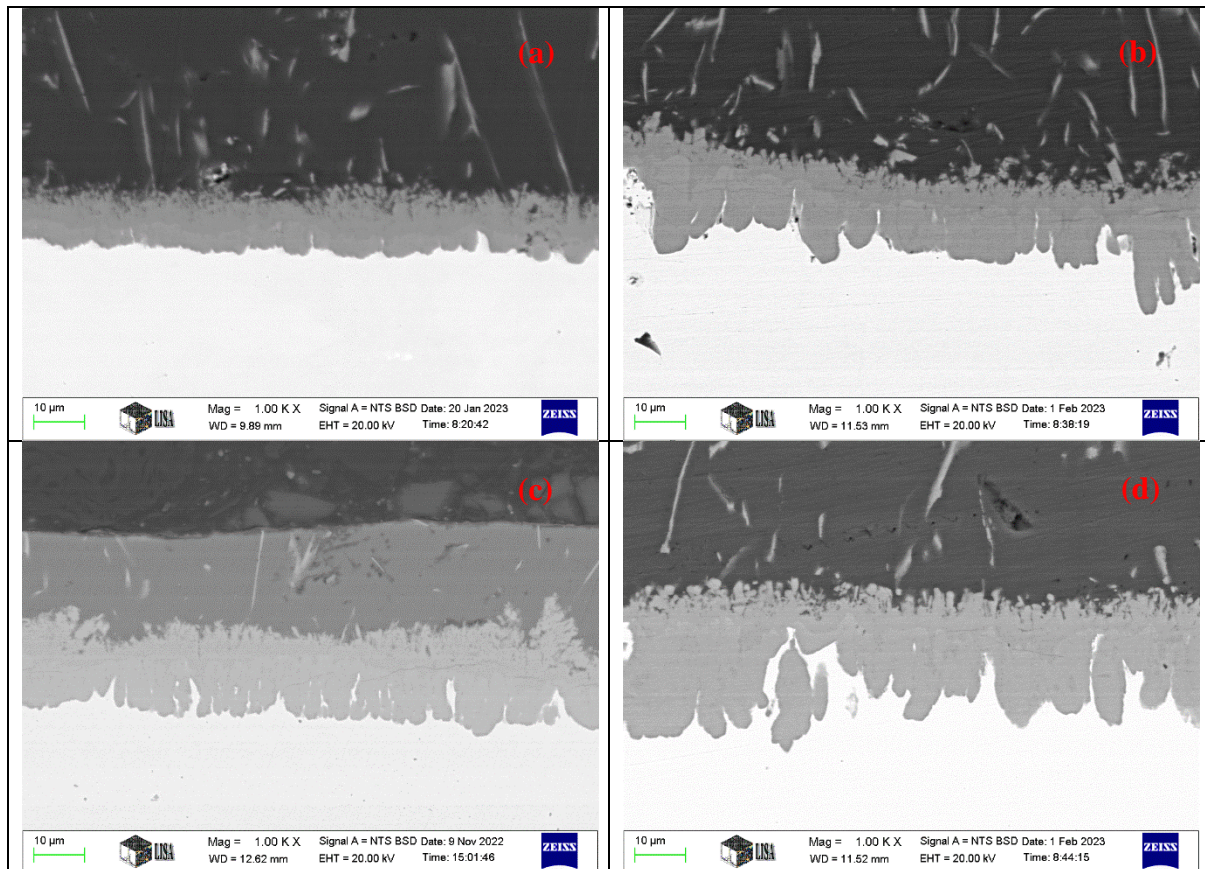


Figure 4. Cross-sectional view of HDA carbon steel C45 pre-coated with copper specimens were dipped in a molten aluminum bath for (a) 43 s, (b) 85 (c) 150 s, and (d) 300 s.

5.3 Oxidation resistance endurance of HDA C45 at elevated temperatures

Oxidation resistance tests were conducted on HDA carbon steel C45 specimens at high temperatures between 700 to 1000 °C for three different exposure periods: 8, 24, and 72 h. The evolution of the oxide scale was charted in Figure 5, displaying the change in weight per surface area versus exposure time.

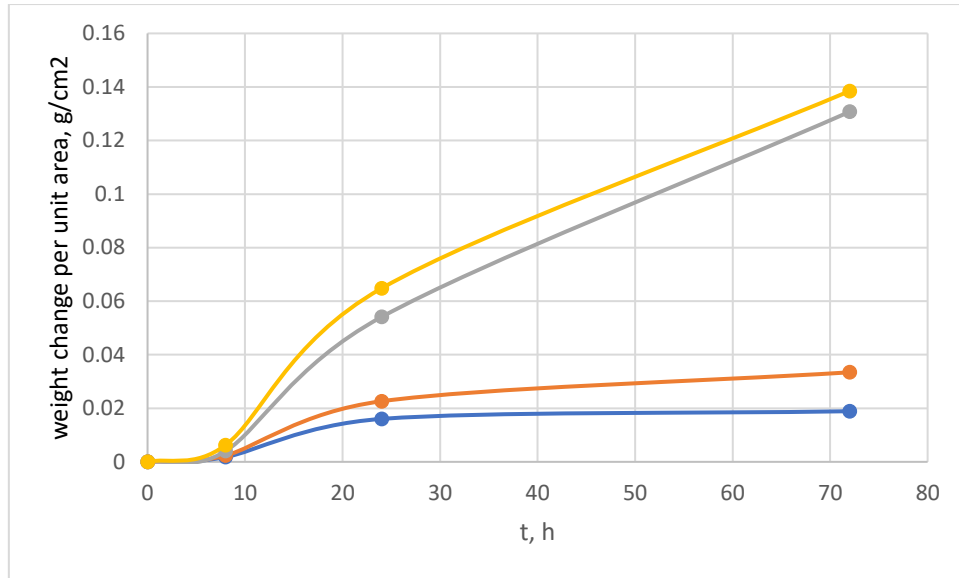


Figure 5. Evolution of oxide scales as a function of weight change per unit area versus time between 700 to 1000 °C.

Between 24 and 72 hours of exposure at 700°C, the scale formation appears to follow a steady state condition without any significant changes. The same pattern is observed for the 800°C exposure, with a slight change in the straightness. At these two temperatures, the HDA specimens exhibit proper resistance to hot air. However, at 900°C and 1000°C, a sharp increase in weight gain is observed between 24 to 72 hours. This indicates that at high temperatures, the aluminized carbon steel C45 is more likely to experience weight gain, suggesting a higher probability of degradation.

Table 2. Growth oxidation kinetic rate for the HDA carbon steel C45 at different temperatures.

Temperature, °C	700	800	900	1000
$k_p, \text{g}^2/\text{cm}^4 \cdot \text{h}^{-1}$	4.73914×10^{-6}	0.00176985	0.004203541	0.00408665

It can be inferred from the results in Table 2 that the oxidation kinetic rate at 900 and 1000 °C is significantly higher than that at 700 °C for HDA carbon steel C45.

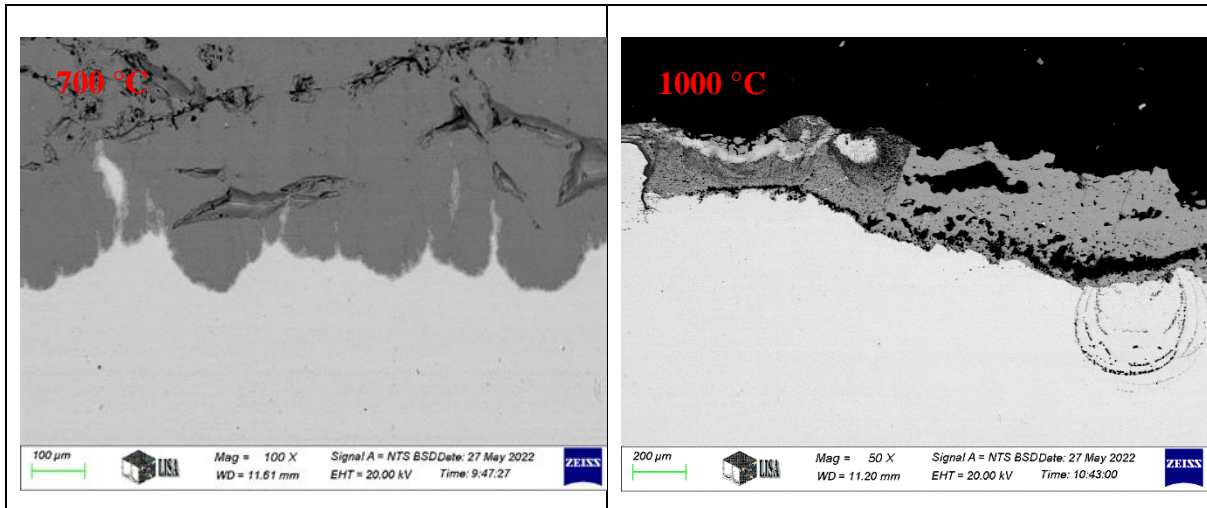


Figure 6. The SEM images show the cross-sections of the HDA samples held for 72 h. The experiment under observation was conducted at a temperature of 1000 °C, resulting in severe sample corrosion and a catastrophic failure of HDA C45. However, the HDA C45 tested at 700 °C did not show such severe corrosion and remains functional.

5.4 Cyclic oxidation resistance of HDA carbon steel C45

The samples exposed to hot air were sectioned and prepared for SEM, EDS, and elemental mapping analyses. A rather thick-coated segment of the HDA specimen surface is shown in Figure 7(a). Several observations can be drawn through the SEM images: with heating, the peak of the tongue or finger-like structure reaching toward the steel substrate became coarser (wider) rather than needle-like. A narrow emergent layer (marked in Figure 7(b)) can clearly be seen between the finger-like structure and the steel substrate (a lighter grey zone). This also fills in the interstices between the finger-like areas and is free of cracks and pores.

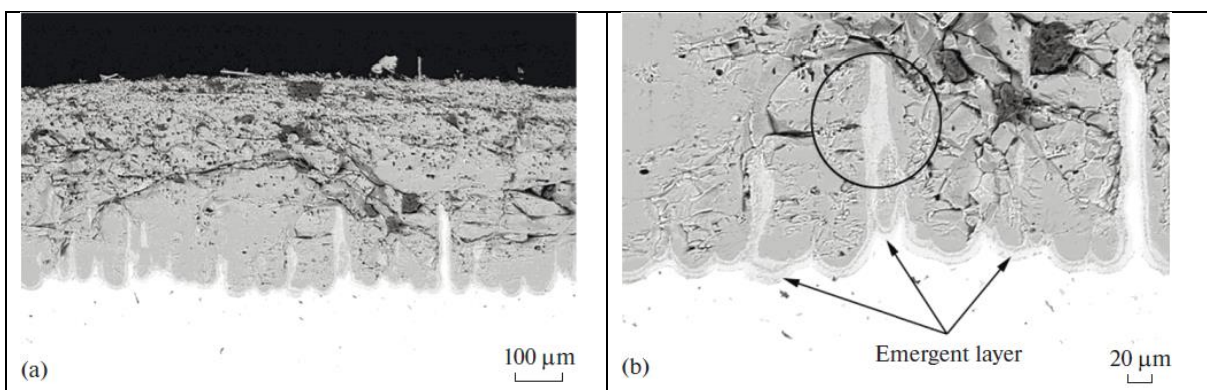


Figure 7. SEM of the aluminized sample after exposure to hot air: (a) cross-section and (b) emergent layer between finger-like structure and steel substrate.

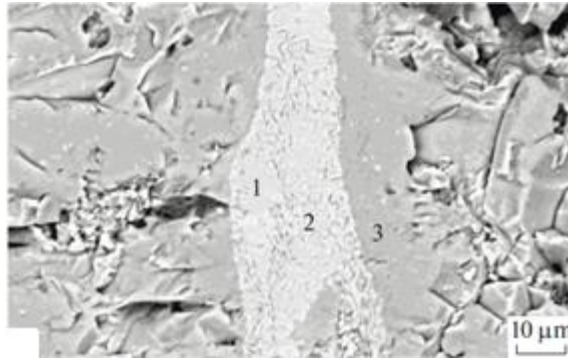


Figure 8. Specified spots in the initiated bright region are marked in Figure. 7(b) by inside circle.

Table 3. Chemical elements detected by EDS spot analysis at different points (Figure 8)

Points no.	Al, at %	Fe, at %	Atomic ratios, Al/Fe	O, at %	Mn, at %
1	45.6	46.6	~1	–	0.42
2	46.51	44.8	~1	–	0.79
3	66.13	28.44	~2	1.58	0.31

5.5 Corrosion resistance of HDA carbon steel C45 half immersed in molten salts

The HDA C45 samples have undergone cutting and preparation procedures for the purpose of metallographic examination. The part that came into direct contact with molten salts has exhibited severe deterioration due to oxychlorination and sulfidation. Both of these factors have accelerated the process of corrosion degradation within the sample and increased with increasing time.

The gradual disappearance of the original finger-like structure of the HDA specimens was observed during high-temperature exposures and after the exposure periods presented in Figure 9(a–f), the distinct surface layers (aluminum topcoat and intermetallic layer) could no longer be observed (as in all cases, it transformed to intermetallics of different kinds). Figure 9(a,b) illustrates the non-immersed and immersed parts of a sample that was exposed for 8 h at 700 °C. In the non-immersed part, many tiny pores are spread throughout the section, whereas in the immersed part, they are mostly concentrated at the top surface in contact with the molten salts (see red arrows). For the samples held for 24 and 72 h, the pores coalesce and produce cracks and grooves that appear to separate two separate layers (see the red arrows in Figure 9(c–f)). There is a distinct color development in the outermost layer for both the 24 and 72 h exposure periods (see the white arrows); this layer has a weak adhesion to the main coat, so parts of it have separated and are easily falling off. It can be seen in Figure 9 that over time,

the interface between the coating layer and the carbon steel substrate C45 becomes nearly flat, as the intermetallics have occupied the gaps within the finger-like structure. Furthermore, as time progressed, the thickness of the coat decreased due to continuous reactions with molten salts or hot air at its outermost layer. The emerging layer (shown in Figure 9 as a light gray zone at the inner interface between the steel and outer intermetallics) also increased in thickness. Furthermore, surface alloying aluminum was also depleted, as part of it was consumed to heal the top protective layer of passive aluminum oxide.

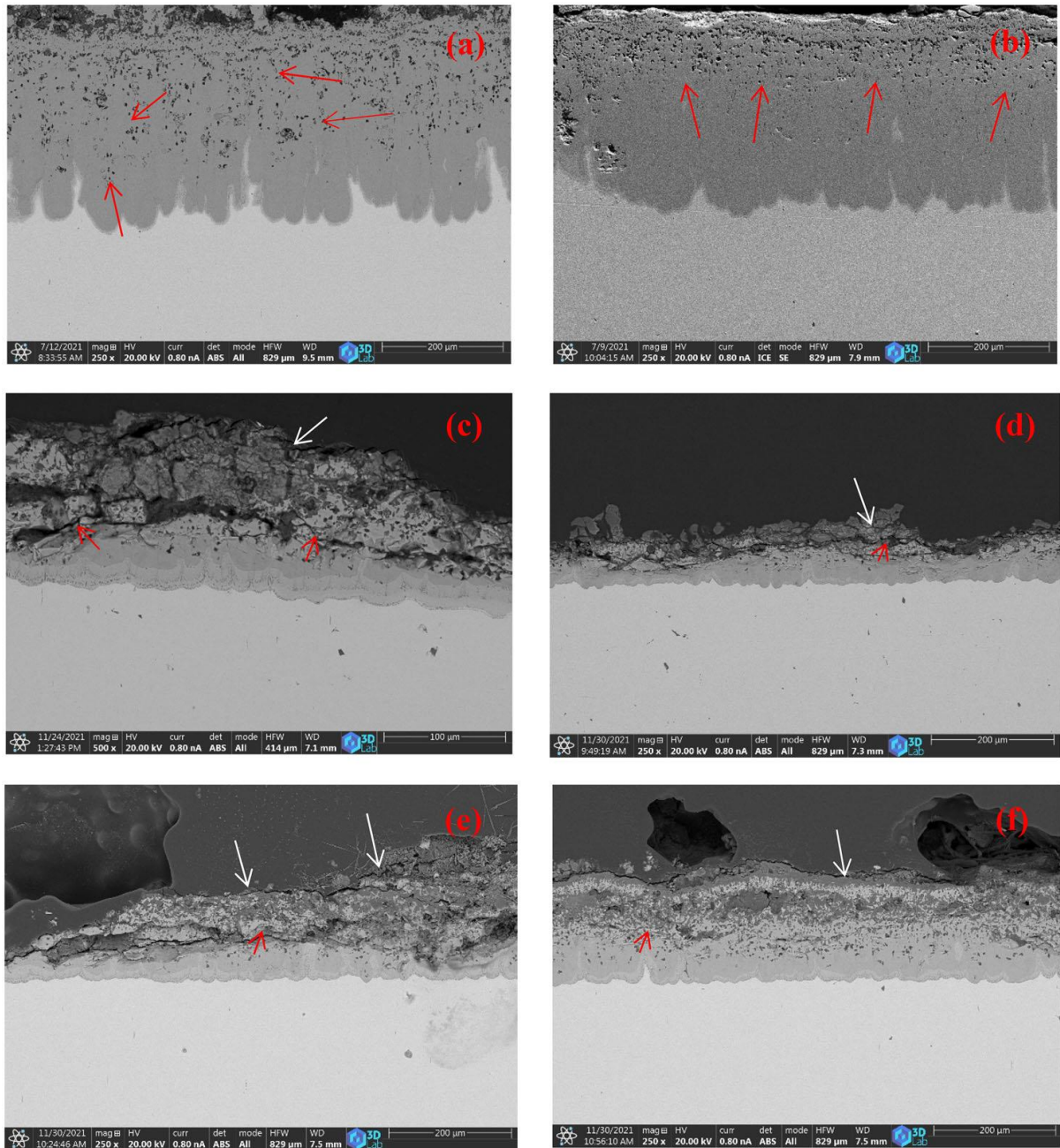


Figure 9. PFIB-SEM cross-section images for both regions in all three samples with different exposure periods of 8 h (a) non-immersed (b) immersed; after 24 h (c) non-immersed (d) immersed, and after 72 h (e) non-immersed (d) immersed.

6. Scientific results

Structure characteristics during hot dip aluminizing and the impact of the interlayer on the intermetallic layer development

Claim 1. The role of carbon content of the substrate steel C45 in the coating layers evolution during hot dip aluminizing with commercially pure aluminium.

During the hot-dip aluminizing (HDA) process run at 700 °C and for 2.5 min dipping time, the iron (Fe) atoms of the solid substrate steel C45 normally tend to diffuse out into the molten aluminum bath and/or produce new solid Fe-Al intermetallics at the solid/liquid interface. This, in turn, should create more vacant places in the steel lattice structure, enhancing the diffusion of some carbon atoms towards the intermetallics and topcoat aluminum layer. Consequently, the structure of the detected EBSD spot (shown in Figures I and II) is similar to that of the perovskite structure of the so-called κ -carbide phase (Fe_3AlC) identified within the intermetallic layer. Whereas the other EBSD spot (shown below on the right) showed a face-centered cubic structure of phase AlC in the topcoat layer. GDOES analysis also confirmed the above findings.

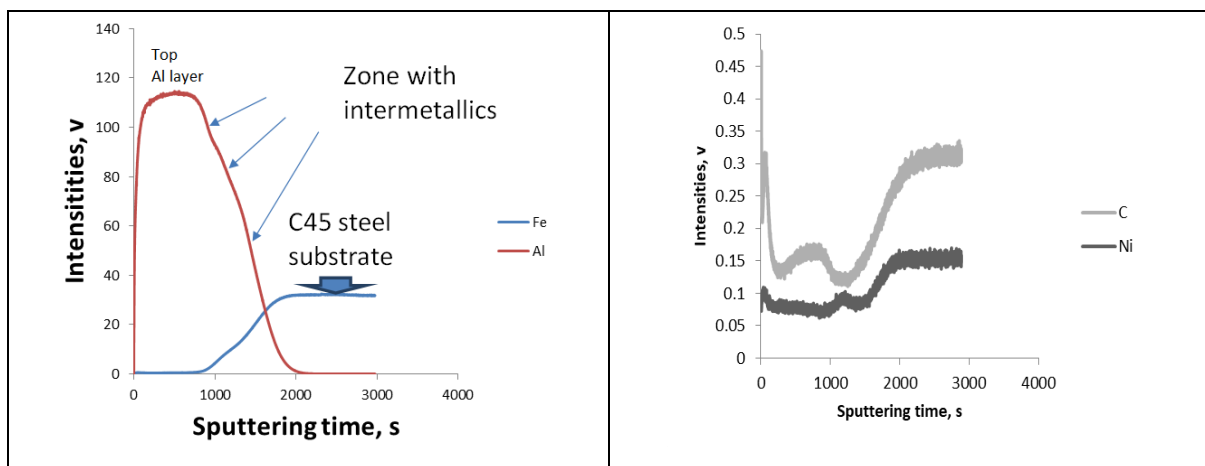


Figure I. GD-OES profiles for Fe and Al, together with the two minor elements C and Ni vs. the argon ion sputtering time, while forming a crater inwards the sample.

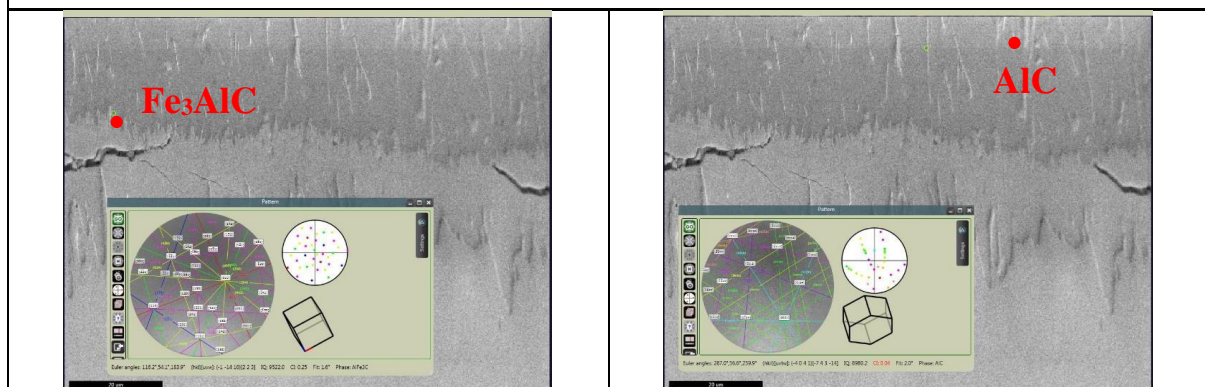


Figure II. The EBSD spot analysis was examined to specify the type of formed phase during HDA.

Claim 2(a)(b). Growth kinetics of Fe_2Al_5 layer due to the copper interlayer before hot dip aluminizing with commercially pure aluminum.

Claim 2(a) Based on my experimental results, I can state that the growth kinetics of $\eta\text{-Fe}_2\text{Al}_5$ follow parabolic growth kinetic with a growth rate equal to $6.46 \times 10^{-13} \text{ m}^2 \cdot \text{s}^{-1}$. The growth rate of $\eta\text{-Fe}_2\text{Al}_5$ has diminished sharply due to using copper as an interlayer before hot dip aluminizing the steel C45 specimens compared with the results of other aluminizing techniques used, such as precoating with other elements or alloying the molten bath (as detailed in Tables I and II).

Claim 2(b) For a short period of immersion of 45 s dipping time, the intermetallic layer thickness amounted to approximately 11 μm , with the $\eta\text{-Fe}_2\text{Al}_5$ layer approximately 4 μm thick and the $\theta\text{-Fe}_4\text{Al}_{13}$ layer approximately 7 μm .

Table I. The intermetallic layer formation characteristics developed on pure and carbon steel substrate during HDA using aluminium alloy as a liquid bath.

Intermetallic Phase type	Bath compositions	Substrate material	Observation based on the structure appearance of the sample's cross-section, including the determined constant growth rate (k)	Dipping time	Aluminizing temperature, °C	Thickness, μm	Ref.
Fe_3Al , Fe_2Al_5 With 6% Si	Al – 1.8 % Si Al – 6 % Si		The interface exhibits a uniform thickness at 1.8% Si content, while with 6% Si, very smooth and planar could be seen at the interface.	2 and 10 min. The structure of both Si-content in liquid baths does not affect by dipping time.	-	~ 20 with 1.8% Si Around 1-2 with 6% Si	[19]
Al-Cu-Fe, Al-Cu	Al – 11 wt.% Cu	AISI 1040	The IM structure displays smooth and even growth for shorter dipping time, while increasing dipping time, uneven growth and a finger-like structure could be seen. The thickness of IM was reduced by up to 75 %.	2-10 min.	700	~ 40 for 2 min. and ~ 50 for 10 min.	[20]
Fe_3Al , Fe_2Al_5 , $\text{Al}_7\text{Fe}_2\text{Si}$, Al_2FeSi , Al_3FeSi_2	Al – 6.9 Si – 1.4 Mg	Interstitial free steel	The IM structure exhibits even, smooth and thin growth, the thickness increased with increasing dipping time.	0.5, 1, 3, and 6 min.	700	~ 25 for 0.5 min., and over 50 for 6 min.	[21]
Fe-Al, Fe-Al-Si	Al – 10 Si	AISI 1005	A continuous, even, and a thin layer of IM formed at the interface.	180 sec.	700	3	[22]
$\text{Fe}_4\text{Al}_{13}$, Fe_2Al_5 At 0% Si up to 4% Si Si from 4% Si $\text{Al}_2\text{Fe}_3\text{Si}_3$ at 6% Si $\text{Al}_8\text{Fe}_2\text{Si}$ at 10% Si, only Fe_2Al_5 and $\text{Al}_8\text{Fe}_2\text{Si}$ exist.	Al – 1, 2, 4, 6, and 10 Wt.% Si	High-purity iron sheet 99.99 Wt.% Fe	The IM layer at 0% Si displays a finger-like structure that starts to transform with the increasing Si content and becomes flattened at 10% Si.	15, 30, 45, 60, 90, 120, 300, 600, 900, 1800 sec.	700	The IM layer thickness at 0% Si equals 66 and becomes around 5 at 10% Si content.	[23]
With 7% Si; $\text{Fe}_2\text{Al}_7\text{Si}$, Fe_2Al_5 , $\text{Fe}_3(\text{Al,Si})_5$, FeAl_3 Same with 12% Si, with 3% Mn Fe_2Al_5 and FeAl_3 and dispersed Mn within the topcoat layer.	Al – 7 Si Al – 12 Si Al – 3 Mn	SAE 1013	The IM layer structure with 7% Si shows a thinner layer in thickness, smooth still the rough (finger-like) structure could be seen but lesser compared to pure aluminium bath and increase slightly with increasing dipping time. In contrast, the bath containing 12% Si had a smoother and flat IM layer growth compared to the previous. The bath, which contains 3% Mn, doesn't show any effect on the structure or the thickness of the intermetallic layer, however, it increases the brittleness of the IM layer, and more cracks could be seen within the IM layer.	5-900 s	750	13 ± 3 for 7% Si 11 ± 5 for 12% Si. The measurement starts from the initial time of dipping till 900 s.	[24]

Fe ₂ Al ₅ and FeAl ₃ with the presence of Si	Al – 8.2 Mg – 4.8 Si	Pure iron	The IM layer exhibit smooth, continuous, thin, and even growth at a certain dipping time and starts to increase slightly.	2 – 1800 s	750		[25]
Fe ₂ Al ₅ , FeAl ₃	Al – 5 Wt.% Cr	Cold-rolled low-carbon steel, 0.036 Wt.%	The structure of IM displayed the same morphology as reported with pure aluminium; it concluded that the chromium has no effect on the intermetallic but improves the scratch hardness due to the presence of Al7Cr dispersed in the top coat layer.	Ranging from 10 to 1800 s.	700	-	[26]
Mainly Fe ₂ Al ₅ , and FeAl ₃ with the presence of a Fe-Al-Si ternary alloy system.	Al – 6.9Si – 1.4Mg	Interstitial-free steel (IF steel)	The IM thickness exhibit smooth, uniform growth and a flat increase in thickness with increasing dipping time.	0.5, 1, 3, and 6 min.	800	Average thickness 4 for 0.5 min. 5 for 1 min. 8 for 3 min. 10 for 6 min.	[27]
-	Al – 1 at.% Si Al – 2 at.% Si Al – 3 at.% Si Al–0.5 at.% Mg Al–1 at.% Mg Al–2 at.% Mg Al–3 at.% Mg	Medium carbon steel 0.44 wt.% C	The IM layer displays uniform growth and is less rough toward the substrate by the addition of Si compared with pure Al bath, and it is increased in thickness with the increasing immersion time. The addition of Mg will return the irregular shape of the IM layer but with less degree compared to pure Al bath. According to the activation energy of 1 at.% Si-Al and 1 at.% Mg-Al, the growth rate is lower compared to pure Al bath.	1, 3, 5, 10, 15, and 20 min.	800	At 1 min. dipping time 3 at.% Si ~ 25 3 at.% Mg ~ 225	[28]

Table II. The intermetallic layer formation characteristics developed on carbon steel substrate during HDA using the precoat method before aluminizing.

Intermetallic Phase type	Bath compositions	Precoat material/ Coating method/Heat treatment	Substrate material	Observation based on the structure appearance of the sample's cross-section, including the determined constant growth rate (k)	Dipping time	Aluminizing temperature, °C	Thickness, μm	Ref.
NiAl ₃ with 5 s, Ni ₂ Al ₃ , NiAl ₃ , (Fe,Ni) ₂ Al ₉ with 60 s, Fe ₂ Al ₅ , FeAl ₃ with 120 s.	Pure aluminium	Nickel/ Electroplating/ without heat treatment	AISI 1005	The IM structure shows even growth for 5 and 30 s dipped time; after longer dipping, i.e., 60 s, the uneven growth starts to appear and clearly could be seen with 120 s dipped time combined with rough growth as a finger-like structure. Growth rate of Fe ₂ Al ₅ layer with n=0.5 was about $6.51 \times 10^{-12} \text{ (m}^2 \cdot \text{s}^{-1}\text{)}$	5-720 s	670	The total IM layer was about 30 with 120 s dipped time.	[29]

Fe ₂ Al ₅ , FeAl ₃	AA 6061	Tin powder + flux (24 g ZnCl ₂ , 6 g NaCl, 3 g NH ₄ Cl, 1 mL HCl and 1 mL H ₂ O)/ powder dispersed in flux mixture/ hot treated on a hot plate for 2.5 min. at 350 °C.	Low-carbon steel, 0.14 Wt.% C.	The IM layer showed even, thin and uniform growth at low dipping time, which increased with increasing time.	0.5, 1, 2.5, and 3.5 min.	750	~ 25 for 0.5 min., and ~ 28 for 2.5 min.	[30]
Fe ₂ Al ₅ , FeAl ₃	Pure aluminium purity 99.7%	Aluminium/ magnetron sputtering/ heat treatment was conducted after deposition for 30 min. at 600 °C in an Ar atmosphere.	Q235	The IM structure exhibits a comb-tooth on the substrate side of the interface, and the neighbouring tooth of the comb-tooth structure was sparsely arranged. The distance between the teeth peak and valley was relatively large.	20 s	720	The average thickness of IM is 9-21, with the mean equal to 15.63 and 3.50 SD.	[31]
Fe ₂ Al ₅ , Fe ₄ Al ₁₃	Commercially pure aluminum 98 %	Copper electroplated	Carbon steel C45	The IM structure exhibits slightly even and regular growth for 45 s dipping time at the interface with the substrate carbon steel C45 then irregular growth with the appearance of a finger-like structure start to grow with increasing dipping time. Growth rate of Fe ₂ Al ₅ layer with n=0.58 was about 0.646 μm ² . s ⁻¹ or (6.46 × 10 ⁻¹³ m ² . s ⁻¹)	45, 85, 150, and 300 s.	700 ± 10 °C	After dipping for 45 s, the IM was about 11 μm, the Fe ₂ Al ₅ was about 4 μm.	Present study

Claim 3. Having compared the difference in grain size between Fe₂Al₅ and Fe₄Al₁₃ phases both for the case of traditional hot dip aluminizing and aluminizing having a copper precoat interlayer.

The average size of about 1.8 μm was achieved for both types of grains at 2.5 min dipping time and a constant aluminizing temperature of 700 °C during the traditional HDA process.

I establish that applying a copper interlayer, which can also form some solid Al-Cu compounds, could hinder the rapid diffusion of both Fe and Al during the first tens of seconds of the dipping process. Hence, it will mitigate the preferential growth in the c-direction of the phase Fe₂Al₅, which will result in getting finer grain than in the case of the traditional HDA process.

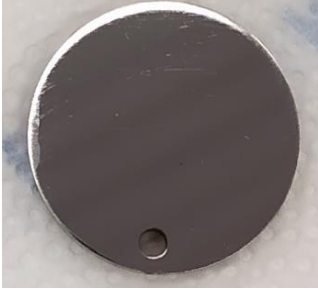



Table III. The difference in grain size of the two main intermetallic phases was obtained with traditional hot dip aluminizing using commercially pure aluminum, and the other obtained after using a precoat layer of copper before hot dip aluminizing.

	Traditional hot dip aluminizing		Using the copper precoat before hot dip aluminizing	
	Fe ₂ Al ₅	Fe ₄ Al ₁₃	Fe ₂ Al ₅	Fe ₄ Al ₁₃
Average grain size	1.8 μm	0.4 μm	1.74 μm	0.75 μm
Std.	1.8	0.075	0.45	0.2

Claim 4. By depositing a thin layer of copper using PVD and applying solder paste-type flux before aluminizing, the wettability of carbon steel C45 can be improved.

Based on experimental observation using PVD and applying paste-type solder flux on the carbon steel C45 before dipping, I can establish that the proper modification of the wettability of carbon steel C45 with our solution (as shown in Table IV) makes it possible to achieve remarkable improvement in the evolution of the aluminized surface layer.

Table IV. Different approaches were used to improve the samples' wettability before aluminizing.

<p>Bare ground and polished carbon steel C45 sample</p>	<p>The aluminized sample was obtained with a salt mixture of KCl, NaCl, and CaF₂ as a flux poured on top of the molten aluminium.</p>	<p>The thickness of carbon steel C45 with thin copper deposited on it via PVD was about one micron.</p>	<p>The aluminized carbon steel C45 was obtained after using the thin copper layer with the addition of a salt mixture of KCl, NaCl, and CaF₂ as a flux poured on top of the molten aluminium.</p>
			

Corrosion resistance of HDA carbon steel C45 in environment with molten salt

Claim 5. The carbon content in the substrate carbon steel C45 and their contribution to the degradation process.

During the high-temperature investigation, I can establish that exposure to molten salt of NaCl and Na₂SO₄ can cause carbon content to accumulate at the interdiffusion layers (emergent layer). It forms a spotty flake-like feature (Figure IV) with different kinds of carbides of the Fe-Al-C system.

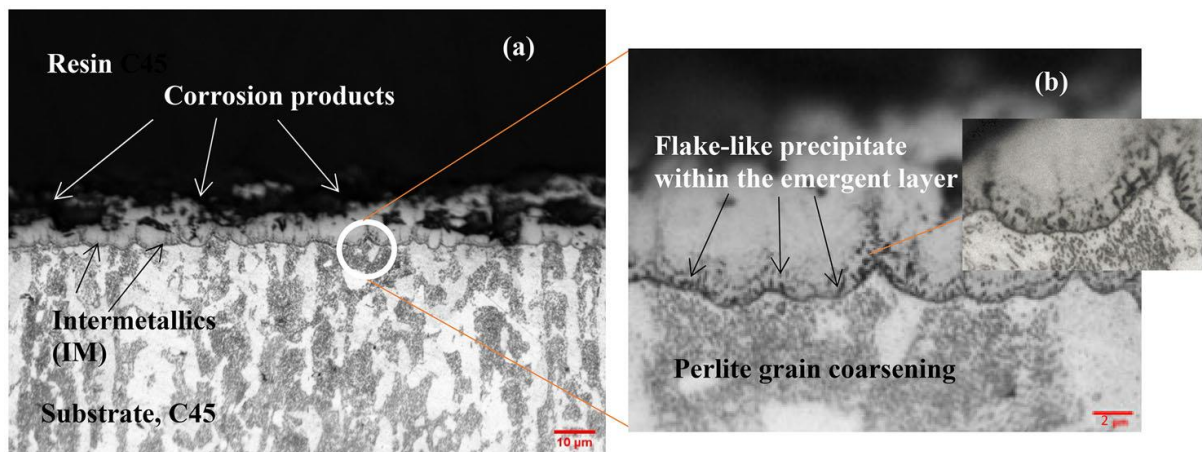


Figure IV. Optical microscope image of HDA half immersed at 700 °C in molten salt with exposure time equal to 24 h; (a) cross-sectional view of the HDA after exposure, (b) the marked portion enlarged to highlight the precipitate of flake-like structure within the emergent layer and the pearlite grain growth/coarsening.

Claim 6. The role of chlorine in the degradation of HDA carbon steel C45 at 700 °C during exposure to molten salt mixture of NaCl and Na₂SO₄ is significant.

Through extensive thermodynamic research, coupled with metallographic analysis, I have discovered the crucial role that chlorine plays in the degradation process by means of cyclic oxychlorination. This finding highlights the importance of understanding and controlling the effects of chlorine in order to improve the durability and performance of such hot dip aluminized (HDA) products.

The oxidation resistance of HDA carbon steel C45 at high temperatures

Claim 7. Suitable temperature for operating HDA carbon steel C45 in hot air environment.

To ensure optimal performance of HDA carbon steel C45 in hot air environment, it has been determined that the hot dip aluminized steel is better operated at a temperature of 700 °C or lower. By doing so, the risk of oxidation and deterioration of the steel substrate is significantly reduced, as demonstrated in Figure V.

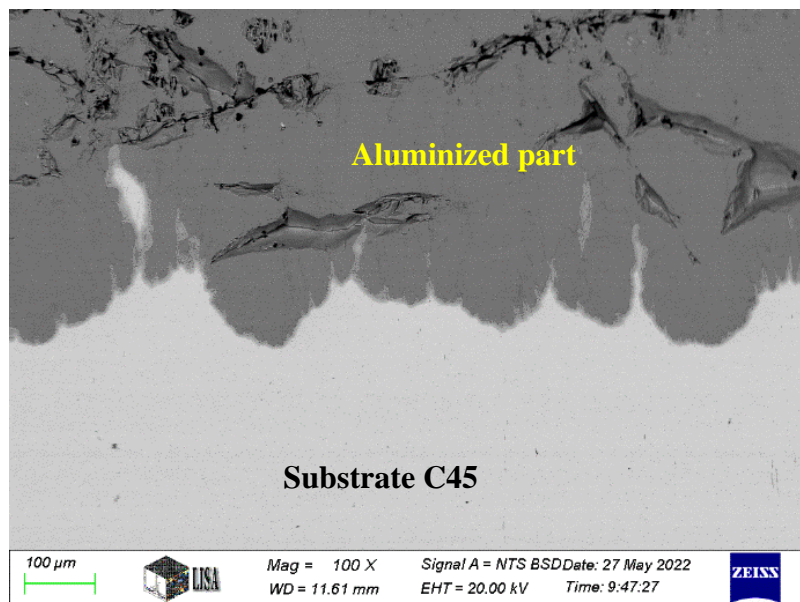


Figure V. The cross-section of HDA carbon steel C45 was held for 72 h at a temperature of 700 °C.

Acknowledgment

I want to give a big shout-out to my supervisor, Prof. Dr. Tamás I. Török, for his exceptional guidance, unwavering support, and invaluable feedback. This work would not have been possible without his assistance, advice, and encouragement. I would like to express my utmost appreciation to my esteemed reviewers and committee, particularly Dr. Zsolt Veres, for thoroughly reviewing my report each semester with great diligence and providing detailed feedback. I extend my sincere gratitude to Mr. Tibor Ferenczi, Mr. Árpád Kovács, Mrs. Anikó Márkus, Mr. Gábor Lassú and Dr. Tibor Kulcsár for their invaluable assistance in the laboratory preparation, material procurement, sample preparation, and conducting laboratory tests including SEM and GD-OES. Their contributions and support were instrumental in the success of my dissertation.

I would like to express my gratitude to Mrs. Ágnes Solczi, Mrs. Zsarnainé Gáthi Gabriella, Mrs. Gabriella Balázsvi-Szabó, and Mrs. Eva Stumpf from the Administration staff. They have been so operative and helpful. Their assistance has been critical in ensuring the smooth running of my Ph.D. program, and I am incredibly thankful for their hard work and dedication.

I also wish to thank the Institute of Chemical Metallurgy and Foundry Engineering and Institute of Physical Metallurgy, Metal Forming, Nanotechnology, Faculty of Materials and Chemical Engineering University of Miskolc, and the Antal Kerpely Doctoral School of Materials Science & Technology (Faculty of Materials Science & Engineering) at the University of Miskolc.

Thanks to the Stipendium Hungaricum Program and the Kurdistan Region Government/Ministry of Higher Education and Scientific Affairs, I was able to study at the University of Miskolc. Finally, I was lucky to meet such talented scientists.

Lastly, I want to express my gratitude to everyone who contributed to this work, even if they were not mentioned here.

List of Publications and conferences

Publications:

1. Hawkar J. Muhammed, Márton Benke, Dániel Koncz-Horváth, Zsolt Sályi, Tamás I. Török. Characterization of Hot-Dip Aluminized C45 Carbon Steel before and after Cyclic Heating in Air, *Surface Engineering and Applied Electrochemistry*. **57**, 431–438 (2021). <https://doi.org/10.3103/S1068375521040116>
2. Hawkar J. Muhammed, Márton Benke, Dániel Koncz-Horváth, Zsolt Sályi, Tamás I. Török, Texture Analysis and Corrosion Testing of Aluminized Carbon Steel C45, *Materials Science and Engineering*, Volume 45, No. 1 (2020), pp. 136–142. DOI: 10.32974.mse.2020.013
3. Hawkar J. Muhammed, Dániel Koncz-Horváth, Gábor Lassú, István Balázs Illés & Tamás I. Török, Characterization Of Fe–Al Intermetallic Phases Formed During Hot-Dip Al Coating on Carbon Steel C45, *MRS Communications* 12, pages 68–73 (2022), <https://doi.org/10.1557/s43579-021-00142-9>.
4. Hawkar J. Muhammed, Dániel Koncz-Horváth, István Balázs Illés & Tamás I. Török, Surface Protective Layers of Iron Aluminides Developed On medium Carbon Steel by The Hot-Dip Aluminizing (HDA) Process, *Multidiszciplináris tudományok*, 11. kötet. (2021) 5 sz. pp.68-77, <https://doi.org/10.35925/j.multi.2021.5.7>.
5. Hawkar J. Muhammed, Dániel Koncz-Horváth & Tamás I. Török, Corrosion Behavior of HDA (Hot-Dip Aluminized) Carbon Steel C45 Half Immersed in Molten Salts (NaCl, Na₂SO₄) Isothermally at 973 K, *Journal of Adhesion Science and Technology*, 13 Dec 2022, <https://doi.org/10.1080/01694243.2022.2159305>

Conferences:

1. Aluminizing (HDA) Process, MultiScience - XXXIV. microCAD International Multidisciplinary Scientific Conference, Miskolc, Hungary, Sep. 2021 <https://multiscience.uni-miskolc.hu/session-programs>.
2. Hawkar J. Muhammed, Dániel Koncz-Horváth, Tamás I. Török, Corrosion behavior of HDA (hot-dip aluminized) carbon steel C45 half immersed in molten salts (NaCl, Na₂SO₄) isothermally at 700 °C, International conference oral presentation, not in Hungarian, Istanbul, Turkey, 25-26 May 2022, <https://casppconferences.com/docs/CaspProgram.pdf>.
3. Oral presentation: Coatings of Turbine Engine Components A review of slurry aluminizing, Ph.D. Forum/ Faculty of Material Science and Technology/ University of Miskolc/ Miskolc/ Hungary, 21.11.2019.

References

- [1] P. R. Roberge, *Handbook of corrosion engineering*, Third. New York: McGraw-Hill, 2019.
- [2] *Uhlig's Corrosion Handbook*. 2011. doi: 10.1002/9780470872864.
- [3] M. G. Fontana, *Corrosion engineering*. New York: McGraw-Hill, 1987.
- [4] N. Birks, G. H. Meier, and F. S. Pettit, *Introduction to the high temperature oxidation of metals, Second edition*, vol. 9780521480420. 2006. doi: 10.1017/CBO9781139163903.

- [5] R. A. Rapp, "High Temperature Oxidation of Metals Forming Cation-Diffusing Scales," *Metallurgical transactions. A, Physical metallurgy and materials science*, vol. 15 A, no. 5, 1984, doi: 10.1007/BF02644552.
- [6] C. J. Wang and J. Y. Pan, "Corrosion of carbon steel with NaCl coating in an atmosphere produced by burning emulsified diesel oil," *Mater Chem Phys*, vol. 82, no. 3, 2003, doi: 10.1016/j.matchemphys.2003.08.017.
- [7] M. Badaruddin, A. Y. E. Risano, H. Wardono, and D. Asmi, "Hot-corrosion of AISI 1020 steel in a molten NaCl/Na₂SO₄ eutectic at 700°C," in *AIP Conference Proceedings*, 2017. doi: 10.1063/1.4968319.
- [8] H. Gerengi, N. Sen, I. Uygur, and E. Kaya, "Corrosion behavior of dual phase 600 and 800 steels in 3.5 wt.% NaCl environment," *J Adhes Sci Technol*, vol. 34, no. 8, 2020, doi: 10.1080/01694243.2019.1688925.
- [9] D. Pradhan, M. Manna, and M. Dutta, "Al-Mg-Mn alloy coating on steel with superior corrosion behavior," *Surf Coat Technol*, vol. 258, 2014, doi: 10.1016/j.surfcoat.2014.08.061.
- [10] D. Lee and X. Xiao, "Corrosion of Fe-17%Cr Steels in (Na₂SO₄+NaCl) Salts at 800 and 900 °C," *Korean Journal of Surface Engineering*, vol. 51, no. 4, 2018.
- [11] C. Ciszak, I. Popa, J. M. Brossard, D. Monceau, and S. Chevalier, "NaCl induced corrosion of Ti-6Al-4V alloy at high temperature," *Corros Sci*, vol. 110, 2016, doi: 10.1016/j.corsci.2016.04.016.
- [12] M. Nimmervoll, A. Schmid, G. Mori, S. Höning, and R. Haubner, "Surface sulphide formation on high-temperature corrosion resistant alloys in a H₂S-HCl-CO₂ mixed atmosphere," *Corros Sci*, vol. 181, 2021, doi: 10.1016/j.corsci.2021.109241.
- [13] Y. F. Yan *et al.*, "Hot corrosion behaviour and its mechanism of a new alumina-forming austenitic stainless steel in molten sodium sulphate," *Corros Sci*, vol. 77, 2013, doi: 10.1016/j.corsci.2013.08.003.
- [14] S. Zhang *et al.*, "Chloride- and sulphate-induced hot corrosion mechanism of super austenitic stainless steel S31254 under dry gas environment," *Corros Sci*, vol. 163, 2020, doi: 10.1016/j.corsci.2019.108295.
- [15] A. C. S. Sabioni, A.-M. Huntz, E. C. da Luz, M. Mantel, and C. Haut, "Comparative study of high temperature oxidation behaviour in AISI 304 and AISI 439 stainless steels," *Materials Research*, vol. 6, no. 2, 2003, doi: 10.1590/s1516-14392003000200012.
- [16] M. Badaruddin, C. J. Wang, Y. Saputra, and A. K. Rivai, "High Temperature Corrosion of Aluminized AISI 4130 Steel with the Different Composition of NaCl/Na₂SO₄ Deposits," *Makara Journal of Technology*, vol. 19, no. 2, 2015, doi: 10.7454/mst.v19i2.3033.
- [17] C.-C. Tsaur, "High temperature oxidation and NaCl-induced accelerated corrosion of hot-dip aluminized 9Cr-1Mo and 310 stainless steel," Doctoral dissertation, Texas A&M University, 2004. Accessed: Nov. 24, 2022. [Online]. Available: <https://hdl.handle.net/1969.1/1375>
- [18] M. Badaruddin, C. J. Wang, H. Wardono, Tarkono, and D. Asmi, "High-temperature oxidation behavior of aluminized AISI 4130 steel," in *AIP Conference Proceedings 1711*, 2016, p. 040002. doi: 10.1063/1.4941624.

- [19] G. H. Awan and F. ul Hasan, "The morphology of coating/substrate interface in hot-dip-aluminized steels," *Materials Science and Engineering: A*, vol. 472, no. 1–2, pp. 157–165, Jan. 2008, doi: 10.1016/j.msea.2007.03.013.
- [20] M. Yousaf, J. Iqbal, and M. Ajmal, "Variables affecting growth and morphology of the intermetallic layer (Fe₂Al₅)," *Mater Charact*, vol. 62, no. 5, pp. 517–525, May 2011, doi: 10.1016/j.matchar.2011.03.004.
- [21] P. P. Dey, P. Modak, A. Ghosh, D. Chakrabarti, P. S. Banerjee, and M. Ghosh, "Investigation of phase evolution of Al–Si–Mg coating on hot dipped interstitial-free steel," *Results in Materials*, vol. 6, p. 100078, Jun. 2020, doi: 10.1016/j.rinma.2020.100078.
- [22] W.-J. Cheng and C.-J. Wang, "Observation of high-temperature phase transformation in the Si-modified aluminide coating on mild steel using EBSD," *Mater Charact*, vol. 61, no. 4, pp. 467–473, Apr. 2010, doi: 10.1016/j.matchar.2010.02.001.
- [23] H. Wang, S. Sun, X. Li, J. Wang, and X. Su, "Effect of silicon on interfacial reaction and morphology of hot-dip aluminizing," *Journal of Materials Research and Technology*, vol. 20, pp. 3723–3734, Sep. 2022, doi: 10.1016/j.jmrt.2022.08.095.
- [24] H. Azimaee, M. Sarfaraz, M. Mirjalili, and K. Aminian, "Effect of silicon and manganese on the kinetics and morphology of the intermetallic layer growth during hot-dip aluminizing," *Surf Coat Technol*, vol. 357, pp. 483–496, Jan. 2019, doi: 10.1016/j.surfcoat.2018.10.035.
- [25] N. Takata, M. Nishimoto, S. Kobayashi, and M. Takeyama, "Morphology and formation of Fe–Al intermetallic layers on iron hot-dipped in Al–Mg–Si alloy melt," *Intermetallics (Barking)*, vol. 54, pp. 136–142, Nov. 2014, doi: 10.1016/j.intermet.2014.06.003.
- [26] P. Huilgol, K. U. Bhat, and K. R. Udupa, "Hot-dip Aluminizing of Low Carbon Steel in Al & Al-5wt % Cr Baths," *Mater Today Proc*, vol. 5, no. 11, pp. 24702–24709, 2018, doi: 10.1016/j.matpr.2018.10.268.
- [27] P. P. Dey *et al.*, "Studies on the characterization and morphological features of the coating on interstitial free steel dipped in molten Al-Si-Mg alloy at 800 °C," *Journal of Materials Research and Technology*, vol. 9, no. 3, pp. 4788–4805, May 2020, doi: 10.1016/j.jmrt.2020.02.104.
- [28] S. K. Kim, "Hot-Dip Aluminizing with Silicon and Magnesium Addition I. Effect on Intermetallic Layer Thickness," *Korean Journal of Metals and Materials*, vol. 51, no. 11, pp. 795–799, Nov. 2013, doi: 10.3365/KJMM.2013.51.11.795.
- [29] W.-J. Cheng and C.-J. Wang, "Characterization of intermetallic layer formation in aluminide/nickel duplex coating on mild steel," *Mater Charact*, vol. 69, pp. 63–70, Jul. 2012, doi: 10.1016/j.matchar.2012.04.007.
- [30] N. Fathy *et al.*, "Influence of Pre-Tinning Process on Coating Morphology and Interface Structure of Low Carbon Steel Dipped in Molten 6061 Al Alloy," *Coatings*, vol. 12, no. 10, p. 1499, Oct. 2022, doi: 10.3390/coatings12101499.
- [31] X. Zhao *et al.*, "Preparation and deformation behaviour of multi-structural aluminium-coated steels," *Surf Coat Technol*, vol. 428, p. 127861, Dec. 2021, doi: 10.1016/j.surfcoat.2021.127861.